

# Methylammonium Lead Iodide Grain Boundaries Exhibit Depth-Dependent Electrical Properties

Gordon A. MacDonald,<sup>a</sup> Mengjin Yang,<sup>b</sup> Samuel Berweger,<sup>c</sup> Jason P. Killgore,<sup>a</sup> Pavel Kabos,<sup>c</sup> Joseph J. Berry,<sup>b</sup> Kai Zhu,<sup>b</sup> Frank W. DelRio<sup>a</sup>

<sup>a</sup>Applied Chemicals and Materials Division, Material Measurement Laboratory,  
National Institute of Standards and Technology, Boulder, CO 80305

<sup>b</sup>National Center for Photovoltaics,  
National Renewable Energy Laboratory, Golden, CO 80401

<sup>c</sup>Applied Physics Division, Physical Measurement Laboratory,  
National Institute of Standards and Technology, Boulder, CO 80305

*Perovskite Film Synthesis:* Methylammonium lead iodide (MAPbI<sub>3</sub>) active layers were deposited as previously reported.<sup>1</sup> Methylammonium iodide (MAI) was purchased from Dyesol, lead iodide (PbI<sub>2</sub>) was obtained from Alfa Aesar, and solvents were purchased from Sigma Aldrich unless otherwise noted. MAI and PbI<sub>2</sub> (1.2:1, molar ratio) were dissolved in a mixture of N-methyl-2-pyrrolidione/ $\gamma$ -butyrolactone (7:3, weight ratio) solvents to form a *ca.* 50 wt% precursor solution. The precursor solution was cast onto either a fluorine-doped tin oxide (FTO)/titanium oxide (TiO<sub>2</sub>) (fabrication described below) or a glass substrate through spin coating at 4500 rpm for 25 s. The substrate was then transferred to a diethyl ether (DEE, Fisher Chemical) bath for *ca.* 90 s. The sample was air dried at room temperature and air annealing on a hotplate, covered by a petri dish, for 15 min at 150 °C.

*Device Fabrication:* FTO substrate (TEC 15, Hartford Glass Co) was patterned using zinc powder and HCl solution as reported previously.<sup>2</sup> Patterned FTO was cleaned prior to the deposition of a compact TiO<sub>2</sub> layer by spray pyrolysis using a 0.2 M titanium diisopropoxide bis(acetylacetonate) in a 1-butanol solution at 450 °C. The TiO<sub>2</sub> layer was annealed at 450 °C for 1 h. The perovskite film was then deposited as described above. A hole transport layer (HTL) was spin coated at 4000 rpm for 30 s with a HTL solution consisting of 80 mg 2,2',7,7'-tetrakis (N, N-dip-methoxyphenylamine)-9,9'-spirobifluorene (Spiro-MeOTAD; Merck), 30  $\mu$ L bis(trifluoromethane) sulfonimide lithium salt (Li-TFSI) stock solution (500 mg Li-TFSI in 1 mL acetonitrile), and 30  $\mu$ L 4-tert-butylpyridine, and 1 mL chlorobenzene solvent. Finally, a 150 nm thick Ag layer was deposited by thermal evaporation through a shadow mask to give a 0.12 cm<sup>2</sup> electrode area.

*Photovoltaic Testing:* The current density (*J*)-voltage (*V*) characteristics were obtained using a 2400 SourceMeter (Keithley) under simulated one-sun AM 1.5G illumination (100 mW·cm<sup>-2</sup>) (Oriel Sol3A Class AAA Solar Simulator, Newport Corporation). A shadow mask (nonreflective metal apertures) with area of 0.12 cm<sup>2</sup> was used to define the active area. Stabilized power output was monitored by a potentiostat (VersaSTAT MC, Princeton Applied Research) near the maximum power output point.

*Scanning Electron Microscopy:* Images were collected with a LEO 1525 field-emission scanning electron microscope. An acceleration voltage of 3 kV was used to minimize electron beam damage.

*Conductive Probe and Photoconductive Atomic Force Microscopy Measurements:* Conductive probe atomic force microscopy (C-AFM) and photoconductive atomic force microscopy (pc-AFM) measurements were performed on an MFP-3D AFM with an ORCA<sup>TM</sup> current sensing module

(Asylum Research). Measurements were performed in a gas purged ( $N_2$ , 99.998 % purity) Humidity Sensing Cell (Asylum Research) using Ir coated AFM probes (Asyelec-01, Asylum Research) with a spring constant ( $k$ )  $\approx 2$  nN/nm. Humidity levels during AFM measurements were typically *ca.*  $2\% \pm 2\%$ . Illumination was achieved from below by focusing a 523 nm LED through a  $50\times$  objective (Olympus) located below the AFM scanning stage. The illuminated area had a diameter of *ca.* 440  $\mu\text{m}$ . Light intensity was calibrated using a Si photodiode. The cantilever detection laser is below the absorption edge for photoexcitation of  $\text{MAPbI}_3$  (wavelength  $\lambda \approx 810$  nm) and does not lead to any measurable photoresponse. Applied forces were calibrated from thermal tune and force curve data and were typically between 30 nN and 170 nN.

**Lateral C-AFM Sample Preparation:** Glass/ $\text{MAPbI}_3$  samples were used for lateral measurements. A razor blade was used to physically remove  $\text{MAPbI}_3$  from part of the sample and the sample was mounted onto a custom stage with an  $11^\circ$  tilt. This ensures that the sample is approximately parallel to a mounted AFM probe chip. A Pt coated AFM probe with  $k \approx 0.2$  nN/nm (ATEC-CONTPt, Nanosensors) was affixed to the AFM head with vacuum grease. A small dab of fast setting epoxy (Double/Bubble Red, Hardman) was then applied to the bottom of the chip and the probe was engaged onto the sample, such that the cantilever extended onto the  $\text{MAPbI}_3$  film and the probe tip was in contact with the  $\text{MAPbI}_3$  film. The epoxy was allowed to cure under a flushed  $N_2$  environment for 1 h. The AFM head was disengaged leaving behind the stationary probe. When close to the sample, the AFM deflection signal would become unreliable. This was due to small shifts in the position and angle of the chip while being weakly held to both the sample by uncured epoxy and to the AFM cantilever holder by vacuum grease. Amplitude *vs.* frequency sweeps were monitored to determine when the probe made contact with the surface (*i.e.* when the resonance peaks shifted from their free values to values associated with the contact resonance frequency of the tip-sample system at a known applied force). This process was used to ensure the probe stayed in contact during the epoxy curing step. These steps were required to minimize damage to the  $\text{MAPbI}_3$  film surface. Electrical contact was made to the probe chip by using silver epoxy (Ted Pella) to affix a copper wire.

**Photovoltaic Device Data:** The aforementioned fabrication process resulted in  $\text{MAPbI}_3$ -based devices with stabilized current density and power conversion efficiency (PCE) of  $19.6 \text{ mA}\cdot\text{cm}^{-2}$  and 17.1 %, respectively. Despite the minor hysteretic behavior, the devices maintained a stabilized PCE of  $> 17\%$ , as shown in Figs. S1a and S1b.

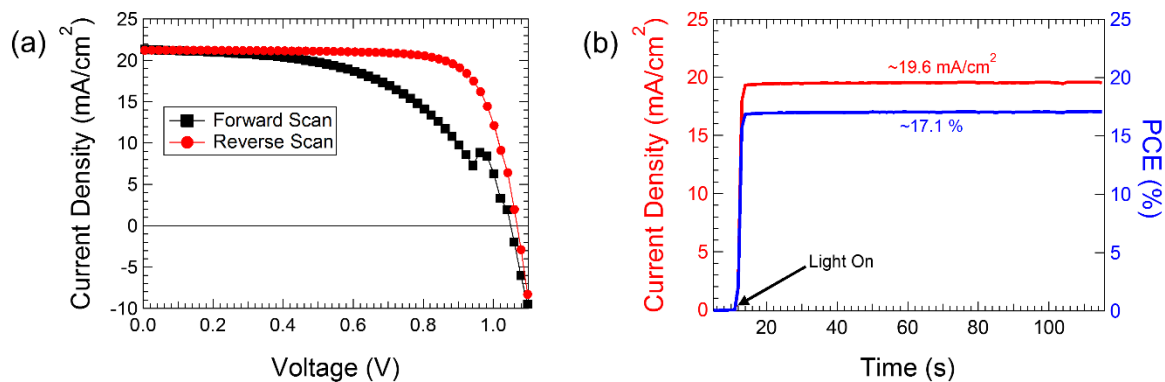


**Fig. S1.** (a) Forward and reverse  $J$ - $V$  scans. The PCE extracted from the max-power-point was 11.9 % and 17.3 % for the forward and reverse scan respectively. (b) The stabilized output of PCE and  $J$  at the max-power-point for FTO/c-TiO/ $\text{MAPbI}_3$ /Spiro-MeOTAD/Ag devices at one-sun illumination.

*Surface Striation C-AFM Measurements:* C-AFM measurements were performed to determine if the striations were limited to a surface effect. As shown in Fig. S2, the striations can be removed by scanning at a sufficient force and/or through repeated scanning in the same location. The force needed to damage the surface depends on several factors, including the “sharpness” of the particular AFM probe. The relative forces needed to induce surface damage are lower for scanning measurements than for stationary force-distance measurements, due to the addition of shear forces while scanning.

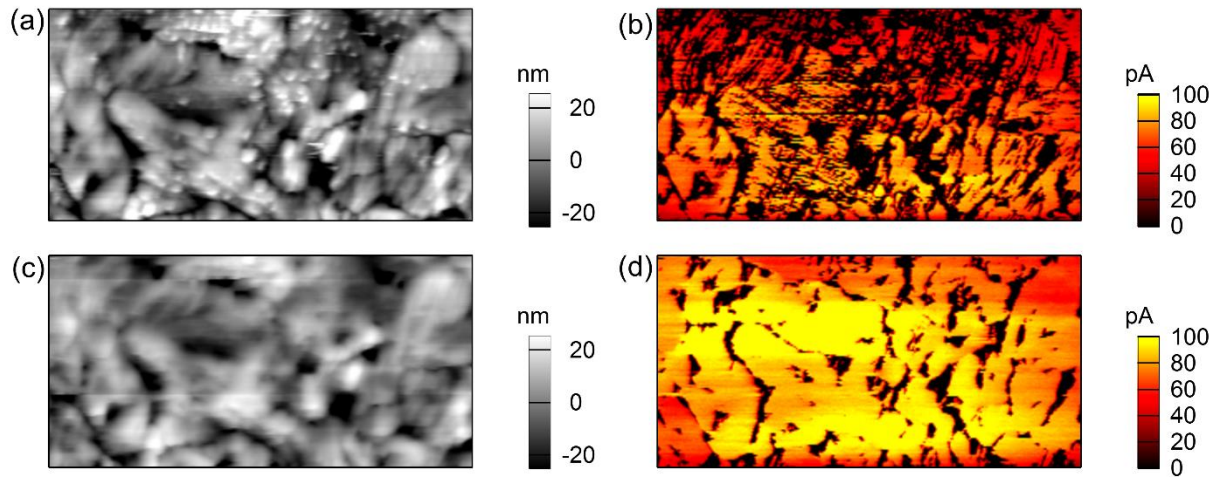


**Fig. S2.** (a) and (c) are topography and (b) and (d) are current data collected at 1.5 V reverse bias and  $\approx 30$  nN applied force. The data collected in (a) and (b) was during the first scan in this area and (c) and (d) was collected during the fourth scan in this same area. Data indicates that resistive regions on individual grains are limited to the top surface and easily removed *via* scanning at modest force. Resistance at grain boundaries (GBs) is not significantly altered under these conditions.

*Scan Direction Artifacts in Lateral Conductivity Measurements:* Fig. S3 establishes that the increased current at GBs often observed in the two-probe conductivity measurements is not due to a greater conductivity at GBs. It is important to first note that this artifact is not due to force overshoot as the probe moves over a feature. If this were the case, the highest current would occur where the deflection or applied force was largest. However, the regions of high current in (c) do not correspond to the regions of greatest deflection error in (b). An alternative explanation is that capacitive charging occurs at the GBs, and is discharged once the probe crosses the GB. This theory is supported by the fact that the highest current spikes correspond to AFM probe movement between a grain that is electrically isolated to a grain that is not electrically isolated, in addition to the fact that the location of the current spike is dependent on the scanning direction.

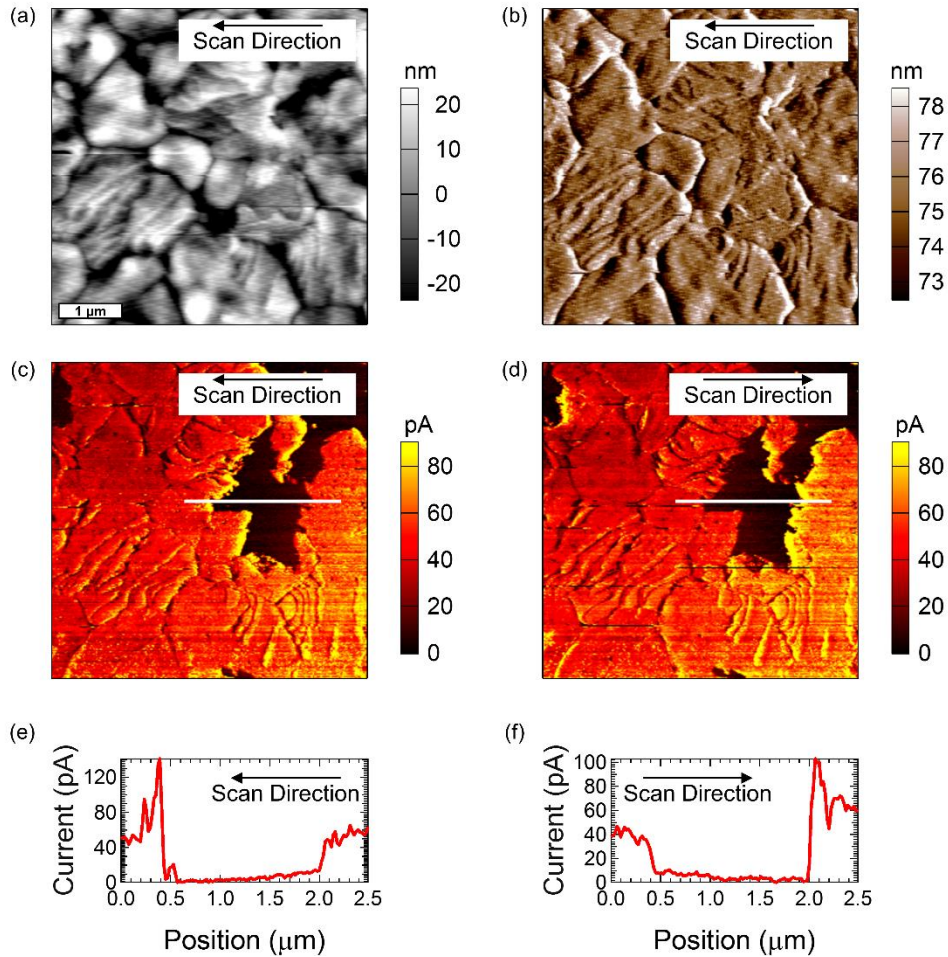


Fig. S3. (a) Height, (b) deflection, and (c) current data from the retrace scan of a lateral conductivity measurement. Current on the trace scan is shown in (d). Line profiles, marked by a white line in (c) and (d), are shown in (e) and (f). The stationary probe is located *ca.* 6.25 μm to the left of the scan location. 10 V was applied between the probe tips and the sample was illuminated with a low level of 523 nm light (*ca.* 0.6 mW·cm<sup>-2</sup>.)

*Impact of Local Surface Potential on C-AFM and pc-AFM Measurements:* The following discussion demonstrates why the variation in the surface potential on MAPbI<sub>3</sub>, observed between GBs and grains, is too small to lead to the large differences (> 2 orders of magnitude) that we observe in current and photocurrent between GBs and grains. For the electrical response to be dominated by the energetic alignment between the metal probe and the semiconducting perovskite film would indicate that a Schottky diode had formed at this junction. Depending on factors such as the applied electric field and the contact area, the current across this nano-Schottky contact will be dominated by either thermionic emission, or by a tunneling current.<sup>3</sup> For responses dominated by thermionic emission, the current across such a junction could be approximated with the ideal diode equation

$$I = I_s \left[ \exp\left(\frac{qV}{kT}\right) - 1 \right]$$

Eq. S1a

where  $I_s$  is described by the following equation

$$I_s = A_d A^{**} T^2 \exp\left(-\frac{\phi}{kT}\right),$$

Eq. S1b

$q$  is the elementary charge,  $V$  is the voltage across the junction,  $k$  is the Boltzman constant,  $T$  is the temperature in Kelvin,  $A_d$  is the active area of the diode,  $A^{**}$  is the Richardson constant for MAPbI<sub>3</sub>, and  $\phi$  is the barrier height between the probe and sample. We can simplify this relationship by only considering the portion related to the barrier height as shown in

$$I \sim \exp\left(-\frac{\phi}{kT}\right)$$

Eq. S2

We can then solve for the relative thermionic emission current on grains ( $I_G$ ) compared to that on GBs ( $I_{GB}$ ), under the assumption that the current response is dominated by the energetic alignment of the probe to the sample,  $\phi_G$  and  $\phi_{GB}$  as follows

$$\frac{I_G}{I_{GB}} \sim \frac{\exp\left(-\frac{\phi_G}{kT}\right)}{\exp\left(-\frac{\phi_{GB}}{kT}\right)}$$

Eq. S3

which is equivalent to

$$\frac{I_G}{I_{GB}} \sim \exp\left(-\frac{\Delta\phi}{kT}\right)$$

Eq. S4

Here  $\Delta\phi$  is the difference in surface potential between GBs and grains. The values reported for  $\Delta\phi$  are typically in the 30 meV to 40 meV range.<sup>1,4,5</sup> Using a value of 40 meV for  $\Delta\phi$  and 300 K for  $T$  results in a ratio of  $I_G$  to  $I_{GB}$  of *ca.* 4.7 under conditions where the current is dominated by thermionic emission. In order to get to a ratio of 100 for  $I_G/I_{GB}$  (*i.e.* two order of magnitude increase in current on grains relative to GBs)  $\Delta\phi$  would need to be *ca.* 110 meV. Thus, the energetic barrier difference

between GBs and grains is too small to lead to the large difference in current in Figs. 2 and 3 under conditions where the current is dominated by thermionic emission.

Similarly, we can explore whether or not the difference in surface potential observed at GBs vs. grains can lead to the difference in current observed, assuming the experiments were performed under conditions that favor tunneling currents. Tunneling currents across nano-Schottky contacts can be described by<sup>3</sup>

$$I = A_d \frac{q^3 E_{max}^2}{8\pi h \varphi} \exp\left(-\frac{8\pi}{3hqE_{max}} (2m^* \varphi^3)^{\frac{1}{2}}\right)$$

Eq. S5

Where  $E_{max}$  is the maximum electrical field at the metal/semiconductor interface,  $h$  is Plank's constant, and  $m^*$  is the effective mass of the majority carrier. This expression can be simplified to a proportionality as shown by

$$I \sim \frac{1}{\varphi} \exp\left(-\varphi^{\frac{3}{2}}\right)$$

Eq. S6

We can then solve for the relative tunneling current on grains ( $I_G$ ) compared to GBs ( $I_{GB}$ ), under the assumption that the current response is dominated by the energetic alignment of the probe and sample,  $\varphi_G$  and  $\varphi_{GB}$  as follows

$$\frac{I_G}{I_{GB}} \sim \frac{\varphi_{GB}}{\varphi_G} \exp(\Delta\varphi^{3/2})$$

Eq. S7

for  $\Delta\varphi = 0.04$  eV (40 meV) the term  $\exp(\Delta\varphi)^{3/2} \approx 1$ . Thus the exponential portion does not significantly impact the ratio of  $I_{GB}$  and  $I_G$  for the experimentally observed values. Thus, we can drop this term, resulting in

$$\frac{I_G}{I_{GB}} \sim \frac{\varphi_{GB}}{\varphi_G}$$

Eq. S8

Furthermore, since the difference between  $\varphi_G$  and  $\varphi_{GB}$  is  $\leq 40$  meV we can rewrite Eq. S8 as follows

$$\frac{I_G}{I_{GB}} \sim \frac{\varphi \pm 40 \text{ meV}}{\varphi}$$

Eq. S9

The term on the right only becomes significant (*i.e.*  $>5$ ) when  $\varphi \leq 10$  meV. However, Kelvin probe force microscope (KPFM) measurements performed with high workfunction probes similar to the ones used in this study (Au, PtIr) show contact potential differences ( $\varphi$ ) between these probes and the surfaces of MAPbI<sub>3</sub> that are greater than 100 meV.<sup>1,4</sup> Thus, this term is not expected to lead to the greater than two order of magnitude difference we observe between  $I_G$  and  $I_{GB}$ .

Since the experimentally observed differences in the surface potential between the GBs and grains is insufficient to lead to the large differences that we observe between  $I_G$  and  $I_{GB}$ , we conclude that the current response in Figs. 2 and 3 is dominated by the local conductivity of the sample rather than due to differences in the energetic alignment of the probe with the sample.

*References:*

- (1) Yang, M.; Zhou, Y.; Zeng, Y.; Jiang, C.-S.; Pature, N. P.; Zhu, K. *Adv. Mater.* **2015**, *27* (41), 6363–6370.
- (2) Zhao, Y.; Zhu, K. *J. Phys. Chem. C* **2014**, *118* (18), 9412–9418.
- (3) Rezeq, M.; Eledlebi, K.; Ismail, M.; Dey, R. K.; Cui, B. *J. Appl. Phys.* **2016**, *120* (4), 044302.
- (4) Yun, J. S.; Ho-Baillie, A.; Huang, S.; Woo, S. H.; Heo, Y.; Seidel, J.; Huang, F.; Cheng, Y.-B.; Green, M. A. *J. Phys. Chem. Lett.* **2015**, *6* (5), 875–880.
- (5) Chen, Q.; Zhou, H.; Song, T.; Luo, S.; Hong, Z.; Duan, H.-S.; Dou, L.; Liu, Y.; Yang, Y. *Nano Lett.* **2014**, *14* (7), 4158–4163.